eNeuro

Research Article: Methods/New Tools | Novel Tools and Methods

Photothrombotic Middle Cerebral Artery Occlusion in mice: a novel model of ischemic stroke

https://doi.org/10.1523/ENEURO.0244-22.2022

Cite as: eNeuro 2023; 10.1523/ENEURO.0244-22.2022

Received: 31 May 2022
Revised: 25 October 2022
Accepted: 6 November 2022

1. Manuscript Title (50 word maximum) Photothrombotic Middle Cerebral Artery Occlusion in mice: a novel model of ischemic stroke

2. Abbreviated Title (50 character maximum) A novel photothrombotic stroke of MCA in mice

3. List all Author Names and Affiliations in order as they would appear in the published article

Emilia Conti[1,2§], Noemi Carlini[1,2], Benedetta Piccardi[3§], Anna Letizia Allegra Mascaro[1,2§†], Francesco Saverio Pavone[2,4,5†]

1 Neuroscience Institute, National Research Council, Via G. Moruzzi 1, 56124 Pisa, Italy.

2 European Laboratory for Non-Linear Spectroscopy, Via Nello Carrara 1, 50019 Sesto Fiorentino, Italy.

3 Neurofarba Department, University of Florence, Viale G. Pieraccini 6, 50139 Florence, Italy.

4 Department of Physics and Astronomy, University of Florence, Via Sansone 1, 50019 Sesto Fiorentino, Italy.

5 National Institute of Optics, National Research Council, Via Nello Carrara 1, 50019 Sesto Fiorentino, Italy.

§ Translational REsEarch on Stroke (TREES) Working Group (in alphabetical order): Allegra Mascaro, A.L., Baldereschi, M., Conti, E., Di Carlo, A.S., Fainardi, E., Kennedy, J., Lombardo, I., Nencini, P., Palumbo, V., Piccardi, B., Sarti, C., Sodero, A., Tudisco, L.

† Equally contributing/last senior authors.

4. Author Contributions:

ALAM conceived the study. EC and NC performed the experiments. EC and NC analyzed the data. EC generated the figures. EC, ALAM, BP wrote the first draft of the manuscript. ALAM, FSP provided funding for the study. All authors contributed to manuscript revision, read, and approved the submitted version.

5. Correspondence should be addressed to (include email address)

Emilia Conti conti@lens.unifi.it

6. Number of Figures: 5
7. Number of Tables: 7
8. Number of Multimedia: 0
9. Number of words for Abstract: 223
10. Number of words for Significance Statement: 111
11. Number of words for Introduction: 421
12. Number of words for Discussion: 1485

13. Acknowledgements: We thank Lapo Turrini (National Institute of Optics, CNR), Claudia Alia (Neuroscience Institute, CNR), and Alessandro Sodero (Neurofarba Department, University of

Florence) for their valuable scientific feedback and discussions. We thank Riccardo Ballerini from the mechanical workshop at LENS for the production of custom pieces.

14. Conflict of Interest

Authors report no conflict of interest

15. Funding sources: This research was funded by the Regione Toscana-Bando Ricerca Salute 2018, Grant number 20RSVP for the project "NIMBLE: Integrating novel NeuroImaging Measurements and circulating Biomarkers for the prediction of secondary injury foLlowing strokE: from bench to bedside", by the Fondazione Cassa di Risparmio di Firenze, Grant number codice SIME 2018/1179 id#24055 for the project "STROKELAB2BED. Ictus ischemico acuto: dal laboratorio al letto del malato. Studio di biomarcatori ematici e di neuroimaging come predittori di edema cerebrale, estensione della lesione ischemica e dell'outcome funzionale", by the European Research Council (ERC) under the European Union's Horizon 2020 research and innovation programme under grant agreement No 692943 (BrainBIT), and by the Bank Foundation Fondazione Cassa di Risparmio di Firenze grant "Human Brain Optical Mapping".

Abstract

Stroke is one of the main causes of death and disability worldwide. Over the past decades, several animal models of focal cerebral ischemia have been developed allowing us to investigate pathophysiological mechanisms underlying stroke progression. Despite intense preclinical research efforts, the need for non-invasive mouse models of vascular occlusion targeting the middle cerebral artery yet avoiding mechanical intervention is still pressing. Here, by applying the photothrombotic stroke model to the distal branch of the middle cerebral artery, we developed a novel strategy to induce a targeted occlusion of a large blood vessel in mice. This approach induces unilateral damage encompassing most of the dorsal cortex from the motor up to the visual regions one week after stroke. Pronounced limb dystonia on day one after the damage is partially recovered after one week. Furthermore, we observe the insurgence of blood vessel leakage and edema formation in the periinfarct area. Finally, this model elicits a strong inflammatory response revealed as a strong increase in astrocytes density and morphological complexity in the perilesional region of the cortex compared to both other regions of the ipsilesional and contralesional hemispheres, and sham-operated mice. To conclude, the stroke model we developed induces in mice the light-mediated occlusion of one of the main targets of human ischemic stroke, the middle cerebral artery, free from the limitations of commonly employed preclinical models.

Significant statement

Cerebral ischemic stroke is one of the leading causes of death and disability worldwide. Animal models represent a fundamental benchmark to investigate the pathophysiological mechanisms underlying stroke patients' outcomes. Here, we developed and characterized a novel mouse model of stroke employing the photothrombotic occlusion of the middle cerebral artery, one of the most common injury sites in stroke patients. The light-mediated occlusion leads in the acute phase to a severe motor deficit accompanied by the insurgence of blood-brain barrier extravasation, and the establishment of an inflammatory regime particularly pronounced in the periinfarct cortex. This simple and highly reproducible model faithfully recapitulates human ischemic stroke avoiding common drawbacks of other stroke models.

Keywords: stroke, MCA photothrombotic occlusion, clasping test, BBB permeability, astrocytes

Introduction

Stroke seriously threatens human health due to its high morbidity, disability, and mortality, thus representing a heavy financial and mental burden affecting families and society (Wafa et al. 2020). Intravenous thrombolysis and endovascular treatment are the standard therapies for patients with acute ischemic stroke. Unfortunately, due to the narrow time window of these treatments, possible treatment inefficacy in terms of recanalization, and the occurrence of reperfusion injury, there is still high variability in determining patients' prognoses. These aspects draw the attention of preclinical research aiming to develop animal stroke models to further elucidate the pathophysiological mechanisms of injury and investigate the main processes of neurovascular disruption. In the past few decades, many strategies have been applied to induce ischemic insult in the brain tissue in animal models. Among the several models developed, middle cerebral artery (MCA) occlusion and photothrombosis are the most diffuse approaches, though characterized by some fundamental drawbacks (Conti et al. 2021; Macrae 2011a).

The intraluminal suture of the middle cerebral artery induces damage in the striatum and cortex, generating a sizable volume of penumbra (Carmichael 2005) with the advantage of avoiding craniotomy and possible brain injury consequent to the surgery (Menzies, Hoff, and Betz 1992; Mies et al. 1991). Nevertheless, MCA occlusion procedures are surgically demanding and may induce local traumatic effects (Kanemitsu et al. 2002). Moreover in this model, the success rate of occlusion and the reproducibility of the infarct size are sometimes unsatisfactory (Yao et al. 2003; Macrae 2011a). On the other hand, the photothrombotic damage shares essential mechanisms occurring with human stroke including the interruption of blood flow due to platelet aggregation and alterations of the blood-brain barrier (BBB) (Dietrich et al. 1987), guaranteeing a high reproducibility between subjects and the capability to easily target the lesioned area (Allegra

Mascaro et al. 2019; Balbi et al. 2017). Nevertheless, this method, widely applied to induce small focal lesions, is poorly employed in large blood vessels that would better represent severe human infarct. Saying that, a search for an occlusion model that encompasses the broad multiplicity of human ischemic progression is still a challenge for preclinical researchers.

Here, we developed and characterized in elderly mice a novel photothrombotic model of the MCA distal branch. We performed *in vivo* evaluations of mice behavior and body weight 24 hours and 7 days after stroke induction. Then, we quantified the extension of the lesion through *ex vivo* immunostaining. Finally, we characterized BBB permeability 24 hours after stroke and alterations of astrocytes morphology through *ex vivo* immunohistochemistry 7 days after photothrombosis.

Materials and Methods

Mice

All procedures involving mice were performed in accordance with regulations of the Italian Ministry of Health. Mice were housed in clear plastic cages under a 12 h light/dark cycle and were given ad libitum access to water and food. We used a transgenic mouse line, C57BL/6J-Tg(Thy1-EGFP)MJrs/J, from Jackson Laboratories (Bar Harbor, Maine USA). 29 Mice were identified by earmarks and numbered accordingly. Animals were randomly divided into 2 groups: stroke (MCAPT n=15; EB n=6) and sham-operated (Sham MCAPT n=4 and Sham EB n=4) mice. To perform the Brain Water Content evaluation and Wire Hanging Behavioral test we employed 8 mice (Sham n=4; MCAPT n=4). Sham-operated mice were subjected to the same surgery and procedure with respect to MCAPT mice except for the Rosebengal injection, replaced by the injection of the same volume of saline. Each group contained comparable numbers of male and female mice. The age of mice (ranging from 16 to 18 months old) was consistent between groups.

Photothrombotic occlusion of the distal branch of the middle cerebral artery

Mice were anesthetized with isoflurane (4% induction, 1.5% maintenance, in 1 L/min oxygen). Body temperature was maintained at 37°C with a heating pad (ThermoStar Temperature Controller, RWD, USA). Mice were placed on a surgery pad, lying on one side. To ensure the stability of the mouse the mouth was secured to the incisor bar and then blocked to the surgery pad. The mouse tail was then tightened to the surgery pad. The muscle over the squamosal bone was stretched with surgical tape to ensure more stability during the surgery. The mouse hairs between the eye and the ear were removed and then the skin was cleaned with betadine and ethanol. Then, local anesthetic lidocaine 2% (20 mg/mL) will be applied. The skin over the squamosal bone was cut, and the muscle was detached from the skull and gently pushed down to expose the bone. We

used a dental drill (Silfradent, Forlì-Cesena Italia) to create a small craniotomy over the squamosal bone to expose the distal branch of the middle cerebral artery. Once removed from the flap bone, a photosensitive dye, Rosebengal (0.2 ml, 10 mg/ml solution in Phosphate Buffer Saline (PBS), was intraperitoneally injected; Sigma Aldrich, USA). To induce photothrombosis, we developed a custom-made setup to finely controlled the laser irradiation on the distal branch of the middle cerebral artery (Fig. 1a). To this aim, we employed a 532 nm laser (Laser Diode CPS532, Thorlabs, Germany) focused with a 70 mm lens onto the targeted blood vessel. The laser intensity at the focus was 128 mW/mm^2 (Watson et al. 2002). The mouse was held by the side on a stage, allowing displacements in the x-y-z directions (Translation Stage DTS25/M, Thorlabs, Germany).

Five minutes after the injection of the dye, ~~a 532 nm~~ green laser was focused before the MCA branch for 25 minutes in order to promote the formation of a stable clot and the consequent occlusion of the distal branch of the MCA. The green laser employed for the experiments focused on the blood vessel and did not heat the irradiated tissue near the MCA during photo-irradiation, as shown by the presence of perfused blood vessels near the illumination site. At the end of the procedure, the muscle will be replaced over the bone and the skin sutured. Mice were placed in their cages until full recovery.

***Ex vivo* evaluation of blood-brain barrier permeability**

To perform an *ex vivo* evaluation of blood-brain barrier permeability we injected in the mouse tail vein 0.20 mL of Evans Blue dye (0.20 mg/mL), at the end of the surgery to occlude the distal branch of the MCA. 24 hours after the injection the animal was anesthetized by an intraperitoneal injection of ketamine (100 mg/kg) and xylazine (10 mg/kg) and then perfused with 100 mL of PBS in order to remove the blood from the brain tissue. The brain was then extracted and in PFA 4% for one hour. Then the brain was sectioned with a brain matrix producing approximately 10 slices 1 mm thick.

Brain water content evaluation

The evaluation of brain water content was performed following the method previously applied by Kenne and collaborators (Kenne et al. 2012). 24 hours after the occlusion of the MCA, mice were sacrificed with an overdose of anesthetic. The brain was divided along the midline and the contralateral and ipsilateral tissue was weighed right after removal to obtain wet weight (WW). The tissue was then dried at 60°C for 72 hours and weighed to obtain dry weight (DW). Water content was calculated as follows: Water Content = (WW-DW)/(DW). Tissue swelling was calculated as a percentage of the ratio between the variation of the wet weight and the initial wet weight: [(Final WW-Initial WW)/(Initial WW)]*100.

Clasping test

The clasping behavior was induced by suspending the mouse from the base of the tail 10 cm above the cage for 20 seconds. We assigned a score of 0 for no clasp if the limbs are splayed outward away from the abdomen. If one limb is retracted towards the stomach for more than 50% of the time suspended we assigned a score of 1. If two limbs are retracted towards the stomach for more than 50% of the time suspended, assigned a score of 2. If three limbs are retracted towards the stomach for more than 50% of the time suspended we assigned a score of 3. If both forelimbs and hindlimbs touch and press on the stomach indicating a severe clasp we assigned a score of 4 (Fig. 2A). At the end of the test, the animal was placed into its cage.

Wire hanging test

To evaluate grip strength, balance, and endurance 24 hours after the injury we tested mice in the wire hanging test (Balkaya et al. 2013). Mice were brought by the tail near a 2 mm thick metallic wire maintained 35 cm above a layer of bedding material to prevent injury to the animal in case of falls. When the animal hung to the wire with the forelimb, the mouse was released by the operator. If the animal reached one end of the wire the score was increased by 1. If the animal fell the score was diminished by 1, and the elapsed time was noted. Mice performed three trials to obtain the final score.

Immunohistochemical analysis

For *ex vivo* investigation, stroke or sham-operated mice were transcardially perfused with 4% paraformaldehyde on day 7 after surgery. Brains were cut using a vibrating-blade vibratome (Leica, Germany) to obtain 100 µm thick coronal sections that were used for immunostaining of Neuronal marker, NeuN (1:1000, anti-NeuN chicken, Millipore, Germany), Glial Fibrillary Acidic Protein, GFAP (1:1000, anti-GFAP rabbit, Abcam, United Kingdom).

The NeuN immunostaining was performed to quantify the lesion volume one week after photothrombosis. The stroke volume for each animal was calculated by summing up all damaged areas and multiplying the number by section thickness and by the spacing factor, 4 (Conti et al. 2022). Images were acquired with a (Stemi 508, Carl Zeiss). The total volume in mm^3 is given as the mean ± standard error of all analyzed animals (n=6). The experimenter was blind to the experimental group of the samples.

The number of Glial Fibrillary Acid Protein (GFAP) positive neurons was analyzed using a confocal fluorescence microscope (Nikon Eclipse TE 300, Tokyo, Japan) with a Nikon Plan EPO 60X objective (NA 1.4, oil immersion Nikon, Tokyo, Japan). We decided to focus our investigation on 4 regions of interest (ROIs), i.e. the peri-infarct area (ischemic border zone, IBZ_{IL}), a region in the ipsilesional

hemisphere distant to the stroke core (remote zone, RZ_{IL}), a region contralateral to the peri-infarct area (ischemic border zone contralateral, IBZ_{CL}), and a region in the healthy hemisphere contralateral to the ischemic core (ischemic core contralateral IC_{CL}). For each ROI (IBZ_{IL}, RZ_{IL}, IBZ_{CL}, IC_{CL}) we acquired 3 fields of view. The density of GFAP positive cells was evaluated considering the following criteria: (i) the same brightness/contrast value was set for all images; (ii) cells placed at the border of the image were not counted; (iii) cells that were not clearly visible were excluded and therefore not counted; (iv) aspecific signals of the background were excluded.

The morphological analysis of astrocytes was performed employing two strategies, i.e. the Sholl method and Skeleton analysis. For each of the 5 animals, 3 slices of the brain, central to the damage, were analyzed. In each slice, we acquired 3 images (212.13x212.13 μm) for each ROI, and in each image, we identified 3 astrocytes. 108 astrocytes per animal were analyzed. We used 4 animals for the analysis of the sham mice. For each animal, we analyzed 3 slices, and for each slice analyzed 3 astrocytes for each of the 4 ROI (IBZ_{IL}, RZ_{IL}, IBZ_{CL}, IC_{CL}). A total of 144 astrocytes were analyzed.

By applying Sholl's method (ImageJ software), we isolated each individual astrocyte and starting from the soma we drew concentric circles around it, at a distance of 3 um from each other. This method allows quantifying the number of intersections of each astrocytic process with a single circumference and the total number of intersections.

We used Skeleton analysis (ImageJ software) to determine the number and length of primary processes, the number of junctions, the number of endpoints, the average length of the processes, and finally the maximum length of the branches of the astrocytes. Since in Sham mice we did not reveal any significant differences between the 4 ROIs we considered a mean value for each parameter in the main figures of the manuscript and we added the Sham analysis for each ROI (IBZ_{IL}, RZ_{IL}, IBZ_{CL}, IC_{CL}) in the Extended data.

Statistical analysis

All the analyses performed of both *in vivo* and *ex vivo* experiments were performed blind. Moreover, all the data were independently evaluated by the two researchers that performed the experiments and the analysis. Results were considered statistically significant if their corresponding P value was less or equal to 0.05. OriginPro software (OriginLab Corporation) was used for all other statistical analyses. For all ANOVAs that were statistically significant, multiple comparisons among time points and different regions of the cortex were assessed using the ANOVA Repeated Measures followed by a post hoc Tukey HSD test.

Results

A novel single-vessel photothrombotic stroke mouse model

We developed a novel method to permanently induce light-mediated occlusion of the distal branch of the middle cerebral artery (MCA) in mice (Fig.1 a, b). The MCA was exposed through a small craniotomy (Fig. 1b left). Then, 5 minutes after the intraperitoneal injection of Rosebengal, the MCA was illuminated for 25 minutes with a green laser (Fig. 1b, middle) which promoted the formation of a stable clot (Fig. 1b, right), and consequently blood perfusion interruption in the downstream brain tissue. We performed the MCA photothrombosis in two different experimental groups (Fig. 1c). In the first one (MCAPT) we performed behavioral experiments the day before the stroke (Pre) and then 24 hours (1dpl) and one week (1wpl) after the photothrombosis. After behavioral evaluations, mice were perfused to perform *ex vivo* experiments. In the second group (EB) mice were tested one day before and one day after stroke. At the end of photothrombosis, we injected in the mouse tail vein Evans Blue, serum albumin binding dye to determine the presence of extravasation (i.e. hemorrhage and edema) in brain tissue one day after damage. For both experimental groups (MCAPT and EB) we performed a set of experiment in which mice were subjected to the same surgery and procedure with respect to MCAPT and EB mice respectively except for the Rosebengal injection, replaced by the injection of the same volume of saline. At the end of the experimental period mice were sacrificed to performed ex vivo evaluations (Fig.1-1). To quantify the lesion volume induced by the photothrombotic occlusion of the MCA one week after stroke, the perfused brain was cut into 100-micron coronal sections. The NeuN immunostaining highlighted a region of dead tissue affecting only the mouse cortex extending from motor regions up to visual areas, in the rostrocaudal direction (Fig. 1d), with an overall lesion volume of 6.9 ± 0.1 mm^3 in stroked mice (Fig. 1e). Sham mice, did not show any sign of tissue suffering due to craniotomy or laser irradiation (see Fig 1-1 from 1 to 4).

MCAPT induces severe dystonia in post-stroke acute phase

In order to assess the functional impairment caused by photothrombosis, we performed the clasping test (Miedel et al. 2017; Guyenet et al. 2010) at different time points (Fig. 2a). While in healthy conditions, all the mice splay the limbs outwards indicating the physiological reflex to grab something when hanged, one day after MCA photothrombosis we observed a considerable worsening of motor performance, only partially recovered one week after stroke (Fig. 2b). Then to better characterize motor performances in the acute phase after stroke, we tested a subgroup of mice in the wire hanging test (MCAPT n=4 and Sham n=4). While the final score remained unaltered 24 hours after the surgery in Sham mice, we observed in MCAPT animals a severe worsening of the grip strength, balance, and endurance (Fig. 2b right panel). Body weight evaluation did not highlight

any significant difference before and after photothrombosis (Fig. 2c), though mice body weight variations are higher in the MCAPT group compared to Sham mice (Fig. 2-1a). The permanent occlusion of the distal branch of the MCA is lethal for 6.6% (n=1) of mice one day after irradiation and 40% (n=5) one week after stroke (Fig. 2d).

MCAPT induces blood-brain barrier leakage and edema formation in the ipsilesional hemisphere

We then wondered if the high percentage of mortality observed during the first week after the MCA occlusion (Fig. 2d) was due to the emergence of blood-brain barrier alterations (i.e. hemorrhage and edema). To clarify this aspect, we used Evans Blue, an organic dye characterized by a very high affinity for serum albumin, which allows a rapid and low-cost assessment of BBB permeability (Saunders et al. 2015). The loss of blood-brain barrier integrity and the consequent extravasation was evaluated by quantifying the presence of blue-staining of cerebral tissue, due to leakage of the dye from the blood vessels to the brain parenchyma (Stoll et al. 2009; Yang et al. 2017). Therefore, in EB mice (n=6), we injected the Evans Blue dye in the mouse tail vein right after photothrombosis. Mice were then sacrificed 24 hours after the injection. While in Sham mice (n=4) no evidence of blood-brain barrier alliteration was revealed (see Fig.1-1, 5-8), in MCAPT mice we observed that the diffusion of the dye affects a large portion of the ipsilesional hemisphere, extending both in the rostral direction up to the olfactory bulbs and in the caudal regions, (Fig. 3a, b). Moreover, the tissue appears to be swollen around the stroke core (Fig. 3a black arrows). These animals, evaluated through the clasping test before (Pre) and one day after stroke (1dpl), showed behavioral deficits comparable to the MCAPT group and no consistent alterations in body weight (Fig. 2-1b, c). In particular, mice with more severe impairment are characterized by a higher extension of extravasation (Fig. 3c). Since this preliminary evaluation suggested the presence of barrier leak, to better quantify the presence of edema 24 hours after the photothrombotic damage we evaluated the brain water content of ipsilesional and contralesional hemispheres as a measure of cerebral edema (Kenne et al. 2012) in another group of mice (Sham n=4, MCAPT n=4). The comparison of the variation of water content between hemispheres of Sham with respect to MCAPT mice showed a significant increase in water after the photothrombotic occlusion of the MCA (Fig. 3d). Moreover, a significant increment of tissue swelling was observed in the MCAPT group, not found in Sham mice (Fig. 3e).

MCAPT increases astrocytes density and complexity in the peri-infarct cortex

To quantify the inflammation induced by the damage, we analyzed astrocytes in different regions of the brain in MCAPT and Sham mice. We identified four regions of interest (Fig 4a) within the cortex: ipsilesional ischemic border zone IBZ_{IL}, remote zone RZ_{IL}, contralesional ischemic border zone IBZ_{CL}, contralesional ischemic core IC_{CL} (see Fig. 4-1). In the ischemic core IC where no fluorescence signal was revealed. At a glance, as shown in Fig. 4b, the IBZ_{IL} in MCAPT animals was characterized by an intense fluorescence signal compared to other regions. The analysis revealed an increase of GFAP-positive astrocytes in the peri-infarct area (IBZ_{IL}) of MCAPT animals with respect to Sham mice (Fig. 4-2). Moreover, astrocyte density in the IBZ_{IL} of MCAPT mice was significantly higher with respect to other regions both in the ipsilesional and the contralesional cortex (Fig. 4c and Tab. 4-1). Then by quantifying the number of branch intersections through Sholl analysis (Fig. 5a), we observed a significant increment of the intersections number (21-27 μm from the cell body) of IBZ_{IL} astrocytes compared to other regions of MCAPT mice (Tab. 5-1). Conversely, in Sham animals, no differences were revealed between the ROIs at increasing distances from the cell body (Fig. 5-1, Tab. 5-2, 5-3). Finally, to further investigate astrocyte morphology, we performed Skeleton analysis to quantify the length of astrocytic processes as well as the number of branches, junctions, and end-points (Fig. 5c, Fig. 5-2). Astrocyte morphology is consistent among all the ROIs in Sham mice (Fig. 5-2b). In detail, astrocytes show a lower number of branches, junctions, and end-point in all the analyzed regions compared to MCAPT mice (Fig. 5c, Fig. 5-2b, Tab. 5-4, 5-5). Conversely, MCAPT mice showed strong differences in morphological features between the regions observed (Fig 5c, Tab. 5-6). In particular, the analysis revealed in the ipsilesional hemisphere a significant difference in the number of branches, junctions, and end-points between IBZ_{IL} and RZ_{IL}. Finally, in the contralesional hemisphere, all morphological parameters were comparable between the two regions analyzed.
This aspect highlights the establishment of an inflammatory regime in the acute phase after stroke involving both hemispheres, though especially prominent in the periinfarct cortex of MCAPT mice.

Discussion

In this study, we adopted the photothrombotic technique to induce an ischemic occlusion of the distal branch of the middle cerebral artery in mice. Despite a similar approach was successful in rats (B. D. Watson et al. 1987), rabbits (B.-Q. Zhao et al. 2002), and in a "tandem occlusion" through the ligation of the common carotid artery in mice (Sugimori et al. 2004), to the best of our knowledge this is the first study showing its application in mice.
The occlusion of the MCA can be achieved with other strategies such as the intraluminal insertion of a filament, the endothelin-1 model, and the ligation or the cauterization of the blood vessel,

resulting in different post-injury complications (Gonzalez and Kolb 2003). As previously discussed, the intraluminal suture of the MCA technique is a widely used animal model of stroke. However, the insertion of the filament leads to obstruction of the hypothalamic artery thus inducing hyperthermia and consequent increase of infarct volume, worsening functional outcome (Q. Zhao et al. 1994; Reglodi et al. 2000). Moreover, this model shows high variability of the infarct size resulting in low reproducibility and an unsatisfactory success rate of occlusion (Howells et al. 2010). Furthermore, the surgery to access and manipulate the vasculature requires skilled and experienced hands (Howells et al. 2010). The endothelin-1 technique is another stroke model commonly employed both in rats and mice, based on the local application of a vasoconstrictor agent. The procedure is easy to perform and allows the control of vessel vasoconstriction modulating the dose of the vasoconstrictive agent. However, this approach is characterized by high variability in stroke volume (Braeuninger and Kleinschnitz 2009). Similarly, the cauterization of the MCA is characterized by low reproducibility (Mora-Lee et al. 2011) and presents several drawbacks, including possible damage to the dura mater and tissue surrounding the vessel. Furthermore, cauterization induces permanent damage, not amenable to reperfusion by removing the suture filament, or by light-induced recanalization thrombolytic agents (Ishrat et al. 2009). Conversely, the photothrombotic model has the advantage of inducing the formation of platelet- and fibrin-rich thrombus in the blood vessels of the irradiated site (Matsuno et al. 1993; Saniabadi et al. 1995). This approach is minimally invasive and is capable to induce highly reproducible cortical damage both in rats and mice, targeting with high precision the location of ischemia (Macrae 2011a). Moreover, photothrombosis has the great advantage of tuning the plasma concentration of the dye, and the intensity and duration of the light in order to control the size and the depth of the lesion. Depending on the procedure applied, the target of photothrombosis ranges from an extended region of the cortex to a single capillary.

In previous studies, the photothrombotic approach was applied to single blood vessels within the mouse brain cortex (Shih et al. 2013). This strategy has on the one hand the advantage of being able to target the region of the damage in order to investigate the microscopic basis of cerebral ischemia, selecting a specific class of blood vessel (i.e. capillary or surface arteriole or venule) in a specific cortical area. By combining the stroke model with imaging setups equipped with multiple light sources, alterations of the vasculature (Sunil et al. 2020; Clark et al. 2019), and brain dynamics, such as cortical depolarizing waves, (Balbi et al. 2017) were monitored *in vivo*.

Here, by characterizing the photothrombotic occlusion of the distal branch of the MCA in mice, we observed the formation of a stable clot in the blood vessel after 25 minutes of laser irradiation that leads to reproducible extended damage in the mouse cortex one week after the lesion. Compared to both single capillary and cortex-targeted photothrombosis, our model, targeting the distal branch of the MCA induces a more severe lesion within the mouse brain cortex. Moreover, with respect to the cortical irradiation model, in which the distribution of pial microvasculature can vary between animals of different ages or strains (Labat-gest and Tomasi 2013), the photothrombotic occlusion of the distal branch of the MCA enables high reproducibility. Furthermore, the model induces a strong behavioral deficit revealed by the clasping and wire hanging tests, mimicking a severe human infarction. Moreover, the MCAPT induces a pronounced leakage of the BBB and edema formation, making it a suitable model to investigate the main consequences affecting human stroke patients i.e. hemorrhagic transformation and cerebral edema. Indeed during the acute phase post-injury, the strong behavioral impairment is accompanied by the alteration of the BBB. Previous studies employing MCA occlusion to induce a cerebral stroke observed an increase in BBB permeability in the acute phase after the damage (Belayev et al. 1996; Rosenberg, Estrada, and Dencoff 1998; Candelario-Jalil, Dijkhuizen, and Magnus 2022). In particular, Fernandez-Lopez and collaborators (Fernandez-Lopez et al. 2012) observed a marked increase in Evans Blue leakage in the injured cortex and in the caudate of adult rats. Moreover, many studies apply magnetic resonance imaging to non-invasively detect BBB leakage and edema after stroke injury (Matsushita et al. 2013; Knight et al. 2008; Taheri et al. 2009) after MCAO.

Finally, a strong upregulation of the glial fibrillary acidic protein (GFAP) was induced, indicating the activation of reactive astrogliosis during the acute phase (Alia et al. 2021; Li et al. 2014). Specifically, the increased density of GFAP-positive cells observed in the peri-infarct cortex of MCAPT mice one week after photothrombosis suggests the beginning of scar formation as previously observed in other studies (Shen et al. 2012; Takamatsu et al. 2002).

Overall the advantages of photothrombotic occlusion of the MCA include the possibility to produce large and consistent infarcts of the cortex, by occluding a large blood vessel through a nonmechanical approach, maintaining the dura mater intact, and the intracranial pressure constant. Although this model requires a craniotomy, one of the main advantages of this method includes the relatively slight invasiveness and the high degree of reproducibility (Yao et al. 2003). Considering the extended edema and the high mortality rate observed, we deem the damage induced by the photothrombotic occlusion of the distal branch of the MCA severe. Indeed our model aims at reproducing a severe stroke, to study the acute consequences due to large vessel occlusion, and the

high mortality observed is due to the high reproducibility of the model. Conversely, in human patients, the pathophysiological insurgence of ischemia is characterized by higher variability both in terms of occlusion site and comorbidities, thus resulting in a wider spectrum of patient's outcomes. However, the photothrombotic model may allow controlling the severity of the injury by tuning the irradiation time and the dye concentration (Macrae 2011). Moreover, our model can also be applied to induce ischemia in neonatal mice. As previously assessed by Maxwell and collaborators (Maxwell and Dyck 2005) the photothrombotic stroke model has several advantages with respect to conventional methods to induce damage in neonatal mice, including transient and permanent MCA occlusion. Indeed, the surgical difficulties of these approaches due to MCA exposure and filament insertion are exacerbated when working with neonatal mice. Conversely, due to the transparency of pup skulls (Jia et al. 2018), the distal branch of the MCA is clearly visible thus avoiding bone thinning or craniotomy for laser irradiation.

Since half of all ischemic strokes occur in MCA territory, the development of a reproducible mouse model of stroke mimicking large thromboembolic stroke in humans is crucial in preclinical animal studies. Moreover, an animal stroke model that better resembles the pathophysiology of human ischemic stroke allows the generation of preclinical datasets suitable for investigating network dynamics and functional biomarkers of post-stroke recovery (Cecchini et al. 2021; Adam et al. 2020; Mascaro et al. 2020; Scaglione et al. 2021; Kreuz et al. 2022). Finally, this approach, to our knowledge never applied in mice, will allow in future experiments the vascular recanalization by illuminating the occluded vessel with a specific wavelength, as previously demonstrated in rats (Brant D. Watson et al. 2002; Yao et al. 2003). The light-induced recanalization will foster the investigation of the neurovascular mechanisms underneath the ischemic progression and will allow testing of neuroprotectant agents such as Glyburide (Sheth et al. 2016, 2018). Indeed previous clinical trials have shown that Glyburide reduces brain swelling after ischemia thus improving patients' survival (Sheth et al. 2014; Simard et al. 2014). In particular, this neuroprotective agent has been proven to be effective in large hemispheric strokes at risk of cerebral edema. Indeed, since our novel stroke model induces alteration of BBB permeability and consequent brain edema, we believe that Glyburide might be an appropriate pharmacological agent to be tested. The photothrombotic occlusion of the distal MCA model was developed thanks to a bi-directional collaborative approach between preclinical and clinical researchers (namely Translational REsEarch on Stroke; TREES Study group). The close collaboration between clinics and research is essential to facilitate the translation of mechanistic insights offered by animal models to the

bedside and to build meaningful experimental studies based on real clinical needs (Conti et al. 2021).

FIGURES

Figure 1. *A novel single-vessel mouse model of photothrombotic stroke: (a) Representative scheme of the custom-made setup for photothrombosis occlusion of the distal branch of the MCA, see methods for details. (b) Representative scheme of the main steps of photothrombotic occlusion of the distal branch of the MCA and corresponding images acquired during surgery. The left panel shows the exposure of the MCA after craniotomy; the middle panel highlights the laser irradiation focused on the blood vessel; the right panel shows the formation of the clot. Scale bar 0.5 mm. (c) Experimental timeline for the two groups MCAPT and EB. (d) Representative brain slices labeled with NeuN antibody. To quantify the lesion volume we analyze one slice every 300 µm. Scale bar 2 mm. The image in the inset, acquired with a confocal microscope, shows a boundary region between the periinfarct cortex and the stroke core. Scale bar 1.25 mm. (e) The right panel shows the quantification (mean ± SEM) of stroke volume for the Sham group (0.1 ± 0.0001) and MCAPT 1 week after photothrombosis (6.9 ± 0.1 mm^3); * p= 2.29E-08 based on one-way ANOVA followed by a post hoc Tukey HSD test (n=6). The error bar for the Sham group (n=4) is below the minimum threshold. See also Figure 1-1.*

Figure 2. *MCAPT induces severe dystonia in the acute phase after stroke: (a) Representative pictures of mice during the clasping test. A score of 0 was assigned to mice with no clasping reflex, 1, 2,3, and 4 were assigned respectively when one, two, three, and four limbs are retracted on the abdomen. (b) Left: The clasping reflex revealed a tendency to higher clasping behavior after stroke both in the acute phase (1dpl) and one week (1wpl) after the insult. * p value based on one-way ANOVA repeated measure followed by a post hoc Tukey HSD test : p Pre-1dpl = 0 ; p Pre-1wpl = 1.57E-05; p 1dpl-1wpl = 0. Right: The wire hanging test revealed a decrease in the strength of mice forelimbs 24 hours after the damage. * p value based on one-way ANOVA repeated measure followed by a post hoc Tukey HSD test : p MCAPT Pre-1dpl = 1.83E-5; p 1dpl Sham-MCAPT = 1.83E-5. (c) The graph shows the mice's weight measured at the three time points. (d) The graph shows the mortality rate 24 hours and one week after the lesion (n=15). See also Figure 2-1.*

Figure 3. *MCAPT induces blood-brain barrier leakage and edema formation in the ipsilesional hemisphere. (a) The upper panels show a dorsal and lateral picture of a representative MCAPT brain of a mouse injected in the tail vein with Evans Blue dye right after photothrombosis. Lower panels (from 1 to 8) show coronal sections of the same animal. Black arrows point to tissue swelling. (b) Ex vivo quantification of the brain tissue presenting blue signal in Sham group and EB group (1dpl) one day after the photothrombotic occlusion. * p=0.003 based on one-way ANOVA followed by a post hoc Tukey HSD test (n=6). (c) The table shows for each EB mouse the Clasping test score and the extension of Extravasation. (d) Brain water content evaluation 24 hours after damage highlights the increase of wet weight in the ipsilesional hemisphere of MCAPT mice with respect to Sham mice. * p=0.003 based on one-way ANOVA followed by a post hoc Tukey HSD test (n=4). (e)Tissue swelling evaluation 24 hours after stroke shows the emergence of brain tissue distortion affecting the*

*ipsilesional hemisphere of MCApt mice. * p=0.0001 based on one-way ANOVA followed by a post hoc Tukey HSD test (n=4).*

Figure 4. *MCAPT increases astrocyte density in the peri-infarct area. (a) A representative brain slice highlighted the ischemic core (IC) and the 4 ROIs identified for the astrocytes analysis. Scale bar 0.5 mm (b) Representative field of view of each ROI acquired with a confocal microscope. Scale bar 45 µm. (c) The graph shows the density (average ± SEM) of GFAP+ cells in the 4 ROIs (IBZ_{IL}= 252.57 ± 33.07; RZ_{IL}= 104.63 ± 13.23; IBZ_{CL}=133.64 ± 29.11; IC_{CL}=115.18 ± 26.894). p value based on one-way ANOVA followed by a post hoc Tukey HSD test, see Table 4-1: p IBZ_{IL}-RZ_{IL} = 0.00721; p IBZ_{IL}-IBZ_{CL} = 0.02508; p IBZ_{IL}-IC_{CL} = 0.01278. See also Figure 4-1 and 4-2.*

Figure 5. *MCAPT increases astrocyte complexity in the peri-infarct area of MCAPT mice. (a) Representative image of an astrocyte analyzed with the Sholl method. (b) The graph shows the distribution of the number of intersections for each radius in the 4 ROIs. p value based on two-way ANOVA Repeated Measures followed by a post hoc Tukey HSD test, see Table 5-1, 5-2, 5-3: radius 7: p IBZ_{IL}-RZ_{IL} = 2.51E-08; p IBZ_{IL}-IBZ_{CL} = 0.006; P IBZ_{IL}-IC_{CL} = 0.006; radius 8: p IBZ_{IL}-RZ_{IL} = 8.65E-07; p IBZ_{IL}-IBZ_{CL} = 0.013; P IBZ_{IL}-IC_{CL} = 1.72E-04: radius 9: p IBZ_{IL}-RZ_{IL} = 6.82E-06; p IBZ_{IL}-IBZ_{CL} = 0.029; P IBZ_{IL}-IC_{CL} = 4.10E-04. (c) Representative image of the same astrocyte in (a) analyzed with the Skeleton analysis. All the features of astrocytes in the 4 ROIs are shown as average ± SEM. The intergroup statistical analysis was performed through a two-way ANOVA Repeated Measures followed by a post hoc Tukey HSD test, see Table 5-4. The intragroup statistical analysis was performed through a one-way ANOVA Repeated Measures followed by a post hoc Tukey HSD test see Table 5-5 and 5-6. Total Branches Lenght Sham= 106.71 ± 3.32;IBZ_{IL}= 176.53 ± 15.04; RZ_{IL}= 128.32 ± 4.74; IBZ_{CL}=152.23 ± 14.49; IC_{cl}=143.28 ± 11.04; intergroup analysis p IBZ_{IL} MCAPT-Sham = 0.002; intragroup analysis p IBZ_{IL}-RZ_{IL} = 0.003; p IBZ_{IL}-IC_{CL} = 0.033. Number of astrocytes Branches Sham= 35.54 ± 1.68; IBZ_{IL}= 54.645 ± 3.126; RZ_{IL}= 43.127 ± 2.161; IBZ_{CL}= 47.307 ± 2.742; IC_{cl}= 47.341 ± 2.113; intergroup analysis p IBZ_{IL} MCAPT-Sham =0.001; intragroup analysis p IBZ_{IL}-RZ_{IL} = 0.044. Number of astrocytes Junctions Sham= 17.18 ± 0.87; IBZ_{IL}= 26.81 ± 1.63; RZ_{IL}= 20.89 ± 1.13; IBZ_{CL}= 23.01 ± 1.421 IC_{cl}= 23.04 ± 1.12; intergroup analysis p IBZ_{IL} MCAPT-Sham = 0.03; intragroup analysis p IBZ_{IL}-RZ_{IL} = 0.026; p IBZ_{IL}-IC_{CL} = 0.042. Number of astrocytes End-points Sham= 18.68 ± 0.77; IBZ_{IL}= 27.47 ± 1.34; RZ_{IL}= 22.49 ± 0.86; IBZ_{CL}= 24.47 ± 1.20; IC_{CL}= 24.58 ± 0.97; intergroup analysis p IBZ_{IL} MCAPT-Sham = 0.02; intragroup analysis p IBZ_{IL}-RZ_{IL} = 0.044. See also Figure 5-1 and 5-2.*

EXTENDED DATA

FIGURES

Figure 1-1. *Sham mice ex-vivo doesn't show sign of tissue suffering. On the right, panels from 1 to 4 show representative coronal brain slices (100 µm thick) labeled with NeuN antibody one week after surgery. The ex vivo analysis does not find regions of tissue suffering or necrosis due to craniotomy or laser irradiation. Scale bar 1 mm. On the left, panels from 5 to 8 show representative coronal brain slices (1 mm thick), 24 hours after surgery and intravenous*

injection of Evans Blue dye. The absence of blue staining highlights that the surgery followed by green laser illumination does not induce BBB permeability alterations.

Figure 2-1. *(a) Body weight evaluation of Sham group at three different time points pre-stroke (Pre), one-day, and one-week post-lesion (1dpl and 1wpl respectively). (b) As observed in MCAPT mice, the clasping reflex revealed a tendency to higher clasping behavior after stroke in the acute phase (1dpl) also in the EB group as well as in the MCAPT. * p value based on one-way ANOVA repeated measure followed by post hoc Tukey's correction: p Pre-1dpl = 0.00002. (c) The body weight monitoring does not highlight any alteration after the MCA occlusion.*

Figure 4-1. *GFAP analysis. Representative images of GFAP-labeled astrocytes in the four different regions of interest (IBZ_{IL}, RZ_{IL}, IBZ_{CL}, IC_{CL}) for each mouse.*

Figure 4-2. *Astrocytes density in Sham mice: On the left, a representative image of anti-GFAP labeled astrocytes, scale bar 45 µm. The graph on the right shows the density (average ± SEM) of GFAP+ cells in the 4 ROIs (IBZ_{IL}= 18 ± 2.2; RZ_{IL}= 17 ± 3.6; IBZ_{CL}= 18 ± 3.1; IC_{CL}= 20.7 ± 5.1).*

Figure 5-1. *Sholl analysis in MCAPT and Sham mice. The graphs show the distribution of the number of intersections for each radius in the 4 ROIs color-coded as in Fig. 5.*

Figure 5-2. *Skeleton analysis of astrocytes in MCAPT (a) and Sham (b) mice: All the parameters evaluated in the 4 ROIs are shown as average± SEM. The intergroup statistical analysis was performed through a two-way ANOVA Repeated Measures followed by a post hoc Tukey HSD test, see Table 5-4. The intragroup statistical analysis was performed through a one-way ANOVA Repeated Measures followed by a post hoc Tukey HSD test see Table 5-5 and 5-6.*
*(a) Junctions (pixel) Sham= 56.37 ± 3.37; IBZ_{IL}= 85.74 ± 4.93; RZ_{IL}= 68.45 ± 3.5; IBZ_{CL}= 74.01 ± 4.36 IC_{CL}= 75.47 ± 4.2; intergroup analysis p IBZ_{IL} MCAPT-Sham = 0.00009. Average Branches Length (*µm*) Sham= 4.28 ± 0.14; IBZ_{IL}= 4.35 ± 0.18; RZ_{IL}= 3.81 ± 0.24; IBZ_{CL}= 4.38 ± 0.18; IC_{CL}= 3.96 ± 0.23; intergroup analysis p IBZ_{IL} MCAPT-Sham = 0.03; intragroup analysis p IBZ_{IL}-RZ_{IL} = 0.01; p IBZ_{CL}-RZ_{IL} = 0.007; IBZ_{CL}-IC_{CL} = 0.05. Maximum Branches Lenght (*µm*) Sham= 14.01 ± 0.37; IBZ_{IL}= 16.11 ± 0.42; RZ_{IL}= 13.95 ± 1.04; IBZ_{CL}= 15.6 ± 1.37; IC_{CL}= 13.53 ± 0.87. (b)Total Branches Lenght Sham= ; IBZ_{IL}= 112.914 ± 9.819; RZ_{IL}= 106.157 ± 5.648 IBZ_{CL}=104.43 ± 6.303 IC_{cl}=193.352 ± 5.869). Number of astrocytes Branches (average ± SEM) in the 4 ROIs (IBZ_{IL}= 40.87 ± 5.15 RZ_{IL}= 34.49 ± 1.7 IBZ_{CL}= 34.05 ± 2.51 IC_{cl}= 32.76 ± 2.84). Number of astrocytes Junctions (IBZ_{IL}= 19.91 ± 2.71 RZ_{IL}= 16.74 ± 0.87 IBZ_{CL}= 16.35 ± 1.29 IC_{cl}= 15.73 ± 1.45). Number of astrocytes End-points in the 4 ROIs (IBZ_{IL}= 21.23 ± 2.28; RZ_{IL}= 17.79 ± 0.84; IBZ_{CL}= 18.19 ± 1.18; IC_{CLl}= 17.519 ± 1.317). Junctions (pixel) (IBZ_{IL}= 67.39 ± 11.48; RZ_{IL}= 54.63 ± 2.02; IBZ_{CL}= 52.56 ± 3.55; IC_{CL}= 50.88 ± 4.79). Average Branches Length (*µm*)(IBZ_{IL}= 3.9 ± 0.15; RZ_{IL}= 4.3 ± 0.25; IBZ_{CL}= 4.37 ± 0.21; IC_{CLl}= 4.54 ± 0.47). Maximum Branches Length µm (IBZ_{IL}= 13.90 ± 0.27; RZ_{IL}= 14.15 ± 0.62; IBZ_{CL}= 14 ± 0.51; IC_{CL}= 14 ± 1.44).*

TABLES

Table 4-1 Astrocytes density intra-group (Sham and MCAPT) and inter groups comparison. One-way ANOVA repeated measure followed by Tukey's test was employed for intra-group comparison. Two-way ANOVA repeated measure followed by Tukey's test was employed for inter-group comparison. Colored cells indicate p-values <0.05.

Table 5-1 Intra-group (MCAPT) comparison of Sholl analysis in different region of the cortex. Two-way ANOVA repeated measure followed by Tukey's test. Colored cells indicate p-values <0.05.

Table 5-2 Intra-group (Sham) comparison of Sholl analysis in different region of the cortex. Two-way ANOVA repeated measure followed by Tukey's test. Colored cells indicate p-values <0.05.

Table 5-3 Inter-group (MCAPT and Sham) comparison of Sholl analysis for each region of the cortex. Two-way ANOVA repeated measure followed by Tukey's test. Colored cells indicate p-values <0.05.

Table 5-4 Inter-group (MCAPT and Sham) comparison of Skeleton analysis for each region of the cortex. Two-way ANOVA repeated measure followed by Tukey's test. Colored cells indicate p-values <0.05.

Table 5-5 Intra-group (Sham) comparison of Skeleton analysis in different region of the cortex. One-way ANOVA repeated measure followed by Tukey's test. Colored cells indicate p-values <0.05.

Table 5-6 Intra-group (MCAPT) comparison of Skeleton analysis in different region of the cortex. One-way ANOVA repeated measure followed by Tukey's test. Colored cells indicate p-values <0.05.

Bibliography

Adam, Ihusan, Gloria Cecchini, Duccio Fanelli, Thomas Kreuz, Roberto Livi, Matteo di Volo, Anna Letizia Allegra Mascaro, et al. 2020. "Inferring Network Structure and Local Dynamics from Neuronal Patterns with Quenched Disorder." *Chaos, Solitons & Fractals*. https://doi.org/10.1016/j.chaos.2020.110235.

Alia, Claudia, Daniele Cangi, Verediana Massa, Marco Salluzzo, Livia Vignozzi, Matteo Caleo, and Cristina Spalletti. 2021. "Cell-to-Cell Interactions Mediating Functional Recovery after Stroke." *Cells* 10 (11). https://doi.org/10.3390/cells10113050.

Allegra Mascaro, Anna Letizia, Emilia Conti, Stefano Lai, Antonino Paolo Di Giovanna, Cristina Spalletti, Claudia Alia, Alessandro Panarese, et al. 2019. "Combined Rehabilitation Promotes the Recovery of Structural and Functional Features of Healthy Neuronal Networks after

599 Stroke." *Cell Reports* 28 (13): 3474–85.e6.
600 Balbi, Matilde, Matthieu P. Vanni, Gergely Silasi, Yuki Sekino, Luis Bolanos, Jeffrey M. LeDue, and
601 Timothy H. Murphy. 2017. "Targeted Ischemic Stroke Induction and Mesoscopic Imaging
602 Assessment of Blood Flow and Ischemic Depolarization in Awake Mice." *Neurophotonics* 4 (3):
603 035001.
604 Balkaya, Mustafa, Jan M. Kröber, Andre Rex, and Matthias Endres. 2013. "Assessing Post-Stroke
605 Behavior in Mouse Models of Focal Ischemia." *Journal of Cerebral Blood Flow and Metabolism:*
606 *Official Journal of the International Society of Cerebral Blood Flow and Metabolism* 33 (3): 330–
607 38.
608 Belayev, L., R. Busto, W. Zhao, and M. D. Ginsberg. 1996. "Quantitative Evaluation of Blood-Brain
609 Barrier Permeability Following Middle Cerebral Artery Occlusion in Rats." *Brain Research* 739
610 (1-2): 88–96.
611 Braeuninger, Stefan, and Christoph Kleinschnitz. 2009. "Rodent Models of Focal Cerebral Ischemia:
612 Procedural Pitfalls and Translational Problems." *Experimental & Translational Stroke Medicine*
613 1 (November): 8.
614 Candelario-Jalil, Eduardo, Rick M. Dijkhuizen, and Tim Magnus. 2022. "Neuroinflammation, Stroke,
615 Blood-Brain Barrier Dysfunction, and Imaging Modalities." *Stroke; a Journal of Cerebral*
616 *Circulation* 53 (5): 1473–86.
617 Carmichael, S. Thomas. 2005. "Rodent Models of Focal Stroke: Size, Mechanism, and Purpose."
618 *NeuroRx: The Journal of the American Society for Experimental NeuroTherapeutics* 2 (3): 396–
619 409.
620 Cecchini, Gloria, Alessandro Scaglione, Anna Letizia Allegra Mascaro, Curzio Checcucci, Emilia Conti,
621 Ihusan Adam, Duccio Fanelli, Roberto Livi, Francesco Saverio Pavone, and Thomas Kreuz.
622 2021. "Cortical Propagation Tracks Functional Recovery after Stroke." *PLoS Computational*
623 *Biology* 17 (5): e1008963.
624 Clark, Taylor A., Colin Sullender, Shams M. Kazmi, Brittany L. Speetles, Michael R. Williamson,
625 Daniella M. Palmberg, Andrew K. Dunn, and Theresa A. Jones. 2019. "Artery Targeted
626 Photothrombosis Widens the Vascular Penumbra, Instigates Peri-Infarct Neovascularization
627 and Models Forelimb Impairments." *Scientific Reports* 9 (1): 2323.
628 Conti, Emilia, Benedetta Piccardi, Alessandro Sodero, Laura Tudisco, Ivano Lombardo, Enrico
629 Fainardi, Patrizia Nencini, Cristina Sarti, Anna Letizia Allegra Mascaro, and Marzia Baldereschi.
630 2021. "Translational Stroke Research Review: Using the Mouse to Model Human Futile
631 Recanalization and Reperfusion Injury in Ischemic Brain Tissue." *Cells* 10 (12).
632 https://doi.org/10.3390/cells10123308.
633 Conti, Emilia, Alessandro Scaglione, Giuseppe de Vito, Francesco Calugi, Maria Pasquini, Tommaso
634 Pizzorusso, Silvestro Micera, Anna Letizia Allegra Mascaro, and Francesco Saverio Pavone.
635 2022. "Combining Optogenetic Stimulation and Motor Training Improves Functional Recovery
636 and Perilesional Cortical Activity." *Neurorehabilitation and Neural Repair*.
637 https://doi.org/10.1177/15459683211056656.
638 Dietrich, W. D., B. D. Watson, R. Busto, M. D. Ginsberg, and J. R. Bethea. 1987. "Photochemically
639 Induced Cerebral Infarction. I. Early Microvascular Alterations." *Acta Neuropathologica* 72 (4):
640 315–25.
641 Fernandez-Lopez, D., J. Faustino, R. Daneman, L. Zhou, S. Y. Lee, N. Derugin, M. F. Wendland, and Z. S.
642 Vexler. 2012. "Blood-Brain Barrier Permeability Is Increased After Acute Adult Stroke But Not
643 Neonatal Stroke in the Rat." *Journal of Neuroscience*. https://doi.org/10.1523/jneurosci.5977-
644 11.2012.
645 Gonzalez, C. L. R., and B. Kolb. 2003. "A Comparison of Different Models of Stroke on Behaviour and
646 Brain Morphology." *The European Journal of Neuroscience* 18 (7): 1950–62.
647 Guyenet, Stephan J., Stephanie A. Furrer, Vincent M. Damian, Travis D. Baughan, Albert R. La Spada,
648 and Gwenn A. Garden. 2010. "A Simple Composite Phenotype Scoring System for Evaluating

649 Mouse Models of Cerebellar Ataxia." *Journal of Visualized Experiments: JoVE*, no. 39 (May).
650 https://doi.org/10.3791/1787.
651 Howells, David W., Michelle J. Porritt, Sarah S. J. Rewell, Victoria O'Collins, Emily S. Sena, H. Bart van
652 der Worp, Richard J. Traystman, and Malcolm R. Macleod. 2010. "Different Strokes for Different
653 Folks: The Rich Diversity of Animal Models of Focal Cerebral Ischemia." *Journal of Cerebral*
654 *Blood Flow and Metabolism: Official Journal of the International Society of Cerebral Blood Flow*
655 *and Metabolism* 30 (8): 1412–31.
656 Ishrat, Tauheed, Iqbal Sayeed, Fahim Atif, and Donald G. Stein. 2009. "Effects of Progesterone
657 Administration on Infarct Volume and Functional Deficits Following Permanent Focal Cerebral
658 Ischemia in Rats." *Brain Research* 1257 (February): 94–101.
659 Jia, Jie-Min, Chuanqi Peng, Yihui Wang, Jie Zheng, and Woo-Ping Ge. 2018. "Control of Occlusion of
660 Middle Cerebral Artery in Perinatal and Neonatal Mice with Magnetic Force." *Molecular Brain*
661 11 (1): 47.
662 Kanemitsu, Hideaki, Tadayoshi Nakagomi, Akira Tamura, Teruaki Tsuchiya, Go Kono, and Keiji
663 Sano. 2002. "Differences in the Extent of Primary Ischemic Damage between Middle Cerebral
664 Artery Coagulation and Intraluminal Occlusion Models." *Journal of Cerebral Blood Flow and*
665 *Metabolism: Official Journal of the International Society of Cerebral Blood Flow and Metabolism*
666 22 (10): 1196–1204.
667 Kenne, Ellinor, Anna Erlandsson, Lennart Lindbom, Lars Hillered, and Fredrik Clausen. 2012.
668 "Neutrophil Depletion Reduces Edema Formation and Tissue Loss Following Traumatic Brain
669 Injury in Mice." *Journal of Neuroinflammation* 9 (January): 17.
670 Knight, Robert A., Yuxia Han, Tavarekere N. Nagaraja, Polly Whitton, Jennifer Ding, Michael Chopp,
671 and Donald M. Seyfried. 2008. "Temporal MRI Assessment of Intracerebral Hemorrhage in
672 Rats." *Stroke; a Journal of Cerebral Circulation* 39 (9): 2596–2602.
673 Kreuz, Thomas, Federico Senocrate, Gloria Cecchini, Curzio Checcucci, Anna Letizia Allegra Mascaro,
674 Emilia Conti, Alessandro Scaglione, and Francesco Saverio Pavone. 2022. "Latency Correction
675 in Sparse Neuronal Spike Trains." Journal of Neuroscience Methods, September, 109703.
676 Labat-gest, Vivien, and Simone Tomasi. 2013. "Photothrombotic Ischemia: A Minimally Invasive and
677 Reproducible Photochemical Cortical Lesion Model for Mouse Stroke Studies." *Journal of*
678 *Visualized Experiments: JoVE*, no. 76 (June). https://doi.org/10.3791/50370.
679 Li, Hailong, Nannan Zhang, Hsin-Yun Lin, Yang Yu, Quan-Yu Cai, Lixin Ma, and Shinghua Ding. 2014.
680 "Histological, Cellular and Behavioral Assessments of Stroke Outcomes after Photothrombosis-
681 Induced Ischemia in Adult Mice." *BMC Neuroscience*. https://doi.org/10.1186/1471-2202-15-
682 58.
683 Macrae, I. M. 2011a. "Preclinical Stroke Research - Advantages and Disadvantages of the Most
684 Common Rodent Models of Focal Ischaemia." *British Journal of Pharmacology*.
685 https://doi.org/10.1111/j.1476-5381.2011.01398.x.
686 ———. 2011b. "Preclinical Stroke Research--Advantages and Disadvantages of the Most Common
687 Rodent Models of Focal Ischaemia." *British Journal of Pharmacology* 164 (4): 1062–78.
688 Mascaro, Anna Letizia Allegra, Egidio Falotico, Spase Petkoski, Maria Pasquini, Lorenzo Vannucci,
689 Núria Tort-Colet, Emilia Conti, et al. 2020. "Experimental and Computational Study on Motor
690 Control and Recovery After Stroke: Toward a Constructive Loop Between Experimental and
691 Virtual Embodied Neuroscience." *Frontiers in Systems Neuroscience*.
692 https://doi.org/10.3389/fnsys.2020.00031.
693 Matsuno, H., T. Uematsu, K. Umemura, Y. Takiguchi, Y. Asai, Y. Muranaka, and M. Nakashima. 1993.
694 "A Simple and Reproducible Cerebral Thrombosis Model in Rats Induced by a Photochemical
695 Reaction and the Effect of a Plasminogen-Plasminogen Activator Chimera in This Model."
696 *Journal of Pharmacological and Toxicological Methods* 29 (3): 165–73.
697 Matsushita, Hideaki, Masanori Hijioka, Akinori Hisatsune, Yoichiro Isohama, Shigeto Iwamoto,
698 Hiroaki Terasawa, and Hiroshi Katsuki. 2013. "MRI-Based Analysis of Intracerebral

699 Hemorrhage in Mice Reveals Relationship between Hematoma Expansion and the Severity of
700 Symptoms." *PloS One* 8 (7): e67691.
701 Maxwell, Kimberley A., and Richard H. Dyck. 2005. "Induction of Reproducible Focal Ischemic
702 Lesions in Neonatal Mice by Photothrombosis." *Developmental Neuroscience* 27 (2-4): 121–26.
703 Menzies, S. A., J. T. Hoff, and A. L. Betz. 1992. "Middle Cerebral Artery Occlusion in Rats: A
704 Neurological and Pathological Evaluation of a Reproducible Model." *Neurosurgery* 31 (1): 100–
705 106; discussion 106–7.
706 Miedel, Christian J., Jennifer M. Patton, Andrew N. Miedel, Edward S. Miedel, and Jonathan M.
707 Levenson. 2017. "Assessment of Spontaneous Alternation, Novel Object Recognition and Limb
708 Clasping in Transgenic Mouse Models of Amyloid-β and Tau Neuropathology." *Journal of*
709 *Visualized Experiments: JoVE*, no. 123 (May). https://doi.org/10.3791/55523.
710 Mies, G., S. Ishimaru, Y. Xie, K. Seo, and K. A. Hossmann. 1991. "Ischemic Thresholds of Cerebral
711 Protein Synthesis and Energy State Following Middle Cerebral Artery Occlusion in Rat." *Journal*
712 *of Cerebral Blood Flow and Metabolism: Official Journal of the International Society of Cerebral*
713 *Blood Flow and Metabolism* 11 (5): 753–61.
714 Mora-Lee, Silvia, Ma Salomé Sirerol-Piquer, María Gutiérrez-Pérez, Tania López, Mayte Casado-
715 Nieto, Carlos Jauquicoam, Gloria Abizanda, et al. 2011. "Histological and Ultrastructural
716 Comparison of Cauterization and Thrombosis Stroke Models in Immune-Deficient Mice."
717 *Journal of Inflammation* 8 (1): 28.
718 Reglodi, D., A. Somogyvari-Vigh, J. L. Maderdrut, S. Vigh, and A. Arimura. 2000. "Postischemic
719 Spontaneous Hyperthermia and Its Effects in Middle Cerebral Artery Occlusion in the Rat."
720 *Experimental Neurology* 163 (2): 399–407.
721 Rosenberg, G. A., E. Y. Estrada, and J. E. Dencoff. 1998. "Matrix Metalloproteinases and TIMPs Are
722 Associated with Blood-Brain Barrier Opening after Reperfusion in Rat Brain." *Stroke; a Journal*
723 *of Cerebral Circulation* 29 (10): 2189–95.
724 Saniabadi, A. R., K. Umemura, N. Matsumoto, S. Sakuma, and M. Nakashima. 1995. "Vessel Wall
725 Injury and Arterial Thrombosis Induced by a Photochemical Reaction." *Thrombosis and*
726 *Haemostasis* 73 (5): 868–72.
727 Saunders, Norman R., Katarzyna M. Dziegielewska, Kjeld Møllgård, and Mark D. Habgood. 2015.
728 "Markers for Blood-Brain Barrier Integrity: How Appropriate Is Evans Blue in the Twenty-First
729 Century and What Are the Alternatives?" *Frontiers in Neuroscience* 9 (October): 385.
730 Scaglione, Alessandro, Emilia Conti, Anna Letizia Allegra Mascaro, and Francesco Saverio Pavone.
731 2022. "Tracking the Effect of Therapy With Single-Trial Based Classification After Stroke."
732 Frontiers in Systems Neuroscience 16 (May): 840922.
733 Shen, Jie, Yoko Ishii, Guihua Xu, Thanh Chung Dang, Takeru Hamashima, Takako Matsushima, Seiji
734 Yamamoto, et al. 2012. "PDGFR-β as a Positive Regulator of Tissue Repair in a Mouse Model of
735 Focal Cerebral Ischemia." *Journal of Cerebral Blood Flow and Metabolism: Official Journal of the*
736 *International Society of Cerebral Blood Flow and Metabolism* 32 (2): 353–67.
737 Sheth, Kevin N., Jordan J. Elm, Bradley J. Molyneaux, Holly Hinson, Lauren A. Beslow, Gordon K. Sze,
738 Ann-Christin Ostwaldt, et al. 2016. "Safety and Efficacy of Intravenous Glyburide on Brain
739 Swelling after Large Hemispheric Infarction (GAMES-RP): A Randomised, Double-Blind,
740 Placebo-Controlled Phase 2 Trial." *Lancet Neurology* 15 (11): 1160–69.
741 Sheth, Kevin N., W. Taylor Kimberly, Jordan J. Elm, Thomas A. Kent, Pitchaiah Mandava, Albert J.
742 Yoo, Götz Thomalla, et al. 2014. "Pilot Study of Intravenous Glyburide in Patients with a Large
743 Ischemic Stroke." Stroke; a Journal of Cerebral Circulation 45 (1): 281–83.
744 Sheth, Kevin N., Nils H. Petersen, Ken Cheung, Jordan J. Elm, Holly E. Hinson, Bradley J. Molyneaux,
745 Lauren A. Beslow, Gordon K. Sze, J. Marc Simard, and W. Taylor Kimberly. 2018. "Long-Term
746 Outcomes in Patients Aged ≤70 Years With Intravenous Glyburide From the Phase II GAMES-
747 RP Study of Large Hemispheric Infarction." *Stroke*.
748 https://doi.org/10.1161/strokeaha.117.020365.

749 Shih, Andy Y., Nozomi Nishimura, John Nguyen, Beth Friedman, Patrick D. Lyden, Chris B. Schaffer,
750 and David Kleinfeld. 2013. "Optically Induced Occlusion of Single Blood Vessels in Rodent
751 Neocortex." *Cold Spring Harbor Protocols* 2013 (12): 1153–60.
752 Simard, J. Marc, Kevin N. Sheth, W. Taylor Kimberly, Barney J. Stern, Gregory J. del Zoppo, Sven
753 Jacobson, and Volodymyr Gerzanich. 2014. "Glibenclamide in Cerebral Ischemia and Stroke."
754 Neurocritical Care 20 (2): 319–33.
755 Stoll, Guido, Christoph Kleinschnitz, Sven G. Meuth, Stefan Braeuninger, Chi Wang Ip, Carsten
756 Wessig, Ingo Nölte, and Martin Bendszus. 2009. "Transient Widespread Blood-Brain Barrier
757 Alterations after Cerebral Photothrombosis as Revealed by Gadofluorine M-Enhanced
758 Magnetic Resonance Imaging." *Journal of Cerebral Blood Flow and Metabolism: Official Journal*
759 *of the International Society of Cerebral Blood Flow and Metabolism* 29 (2): 331–41.
760 Sugimori, Hiroshi, Hiroshi Yao, Hiroaki Ooboshi, Setsuro Ibayashi, and Mitsuo Iida. 2004. "Krypton
761 Laser-Induced Photothrombotic Distal Middle Cerebral Artery Occlusion without Craniectomy
762 in Mice." *Brain Research. Brain Research Protocols* 13 (3): 189–96.
763 Sunil, Smrithi, Sefik Evren Erdener, Blaire S. Lee, Dmitry Postnov, Jianbo Tang, Sreekanth Kura,
764 Xiaojun Cheng, Ichun Anderson Chen, David A. Boas, and Kıvılcım Kılıç. 2020. "Awake Chronic
765 Mouse Model of Targeted Pial Vessel Occlusion via Photothrombosis." *Neurophotonics* 7 (1):
766 015005.
767 Taheri, Saeid, Eduardo Candelario-Jalil, Eduardo Y. Estrada, and Gary A. Rosenberg. 2009.
768 "Spatiotemporal Correlations between Blood-Brain Barrier Permeability and Apparent
769 Diffusion Coefficient in a Rat Model of Ischemic Stroke." *PloS One* 4 (8): e6597.
770 Takamatsu, Hiroyuki, Mitsuyoshi Tatsumi, Satoshi Nitta, Rikiya Ichise, Kouji Muramatsu, Masatoshi
771 Iida, Shintaro Nishimura, and Kazuo Umemura. 2002. "Time Courses of Progress to the Chronic
772 Stage of Middle Cerebral Artery Occlusion Models in Rats." *Experimental Brain Research.*
773 *Experimentelle Hirnforschung. Experimentation Cerebrale* 146 (1): 95–102.
774 Wafa, Hatem A., Charles D. A. Wolfe, Eva Emmett, Gregory A. Roth, Catherine O. Johnson, and
775 Yanzhong Wang. 2020. "Burden of Stroke in Europe: Thirty-Year Projections of Incidence,
776 Prevalence, Deaths, and Disability-Adjusted Life Years." *Stroke; a Journal of Cerebral Circulation*
777 51 (8): 2418–27.
778 Watson, B. D., W. D. Dietrich, R. Prado, and M. D. Ginsberg. 1987. "Argon Laser-Induced Arterial
779 Photothrombosis. Characterization and Possible Application to Therapy of Arteriovenous
780 Malformations." *Journal of Neurosurgery* 66 (5): 748–54.
781 Watson, Brant D., Ricardo Prado, Alexander Veloso, J-P Brunschwig, and W. Dalton Dietrich. 2002.
782 "Cerebral Blood Flow Restoration and Reperfusion Injury After Ultraviolet Laser–Facilitated
783 Middle Cerebral Artery Recanalization in Rat Thrombotic Stroke." *Stroke*.
784 https://doi.org/10.1161/hs0202.102730.
785 Yang, Jie, Qian Li, Zhongyu Wang, Cunfang Qi, Xiaoning Han, Xi Lan, Jieru Wan, et al. 2017.
786 "Multimodality MRI Assessment of Grey and White Matter Injury and Blood-Brain Barrier
787 Disruption after Intracerebral Haemorrhage in Mice." *Scientific Reports* 7 (January): 40358.
788 Yao, Hiroshi, Hiroshi Sugimori, Kenji Fukuda, Junichi Takada, Hiroaki Ooboshi, Takanari Kitazono,
789 Setsuro Ibayashi, and Mitsuo Iida. 2003. "Photothrombotic Middle Cerebral Artery Occlusion
790 and Reperfusion Laser System in Spontaneously Hypertensive Rats." *Stroke; a Journal of*
791 *Cerebral Circulation* 34 (11): 2716–21.
792 Zhao, Bing-Qiao, Yasuhiro Suzuki, Kazunao Kondo, Ken-Ichi Kawano, Yasuhiko Ikeda, and Kazuo
793 Umemura. 2002. "A Novel MCA Occlusion Model of Photothrombotic Ischemia with Cyclic Flow
794 Reductions: Development of Cerebral Hemorrhage Induced by Heparin." *Brain Research. Brain*
795 *Research Protocols* 9 (2): 85–92.
796 Zhao, Q., H. Memezawa, M. L. Smith, and B. K. Siesjö. 1994. "Hyperthermia Complicates Middle
797 Cerebral Artery Occlusion Induced by an Intraluminal Filament." *Brain Research* 649 (1-2):
798 253–59.

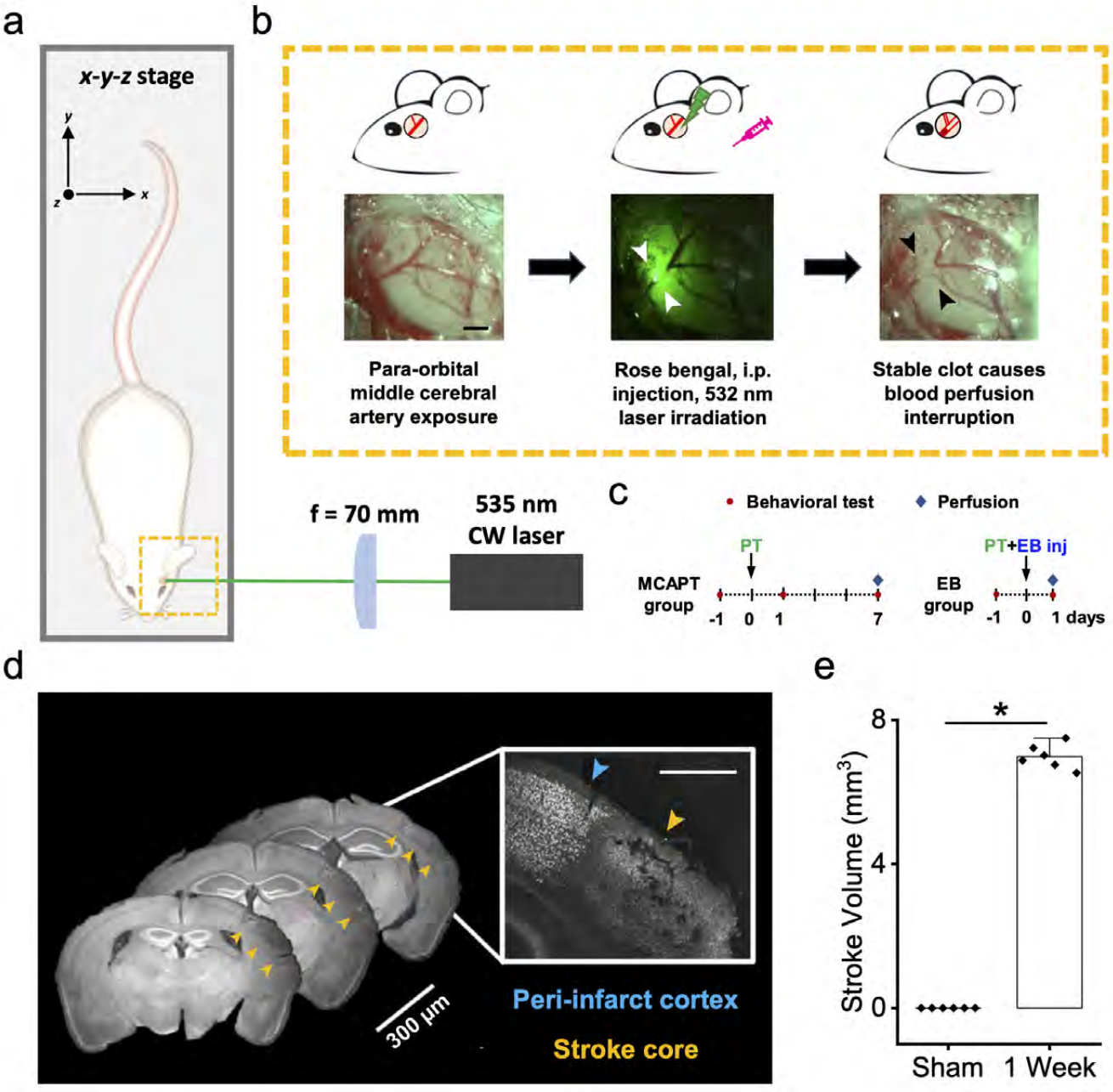

a

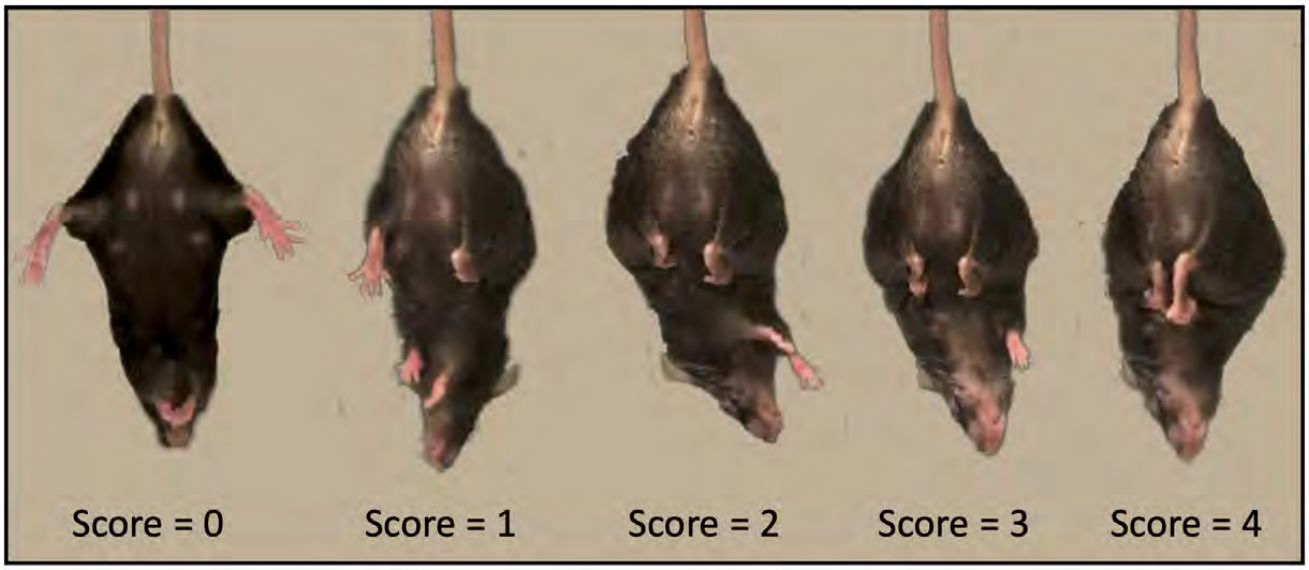

b

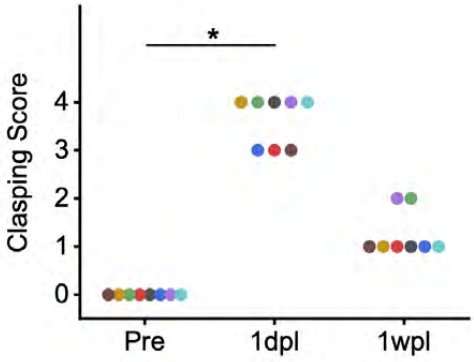

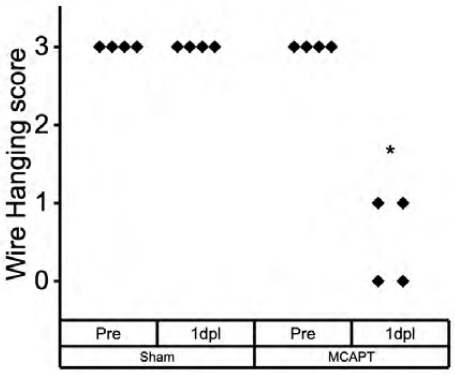

c

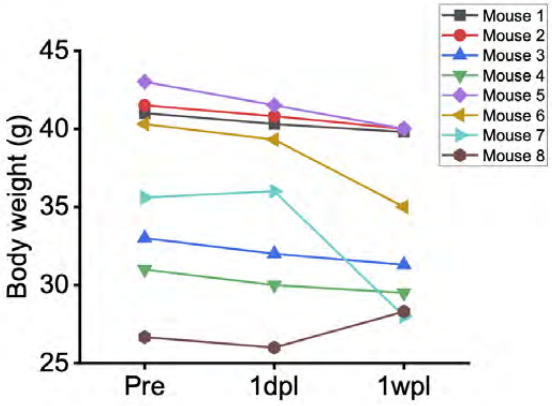

d

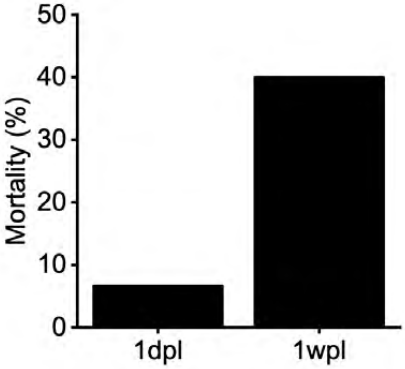

a

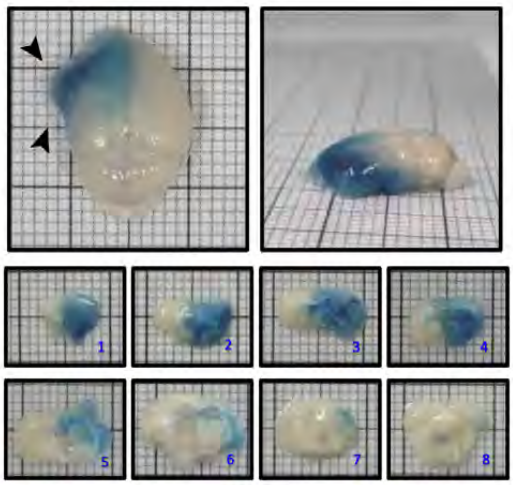

b

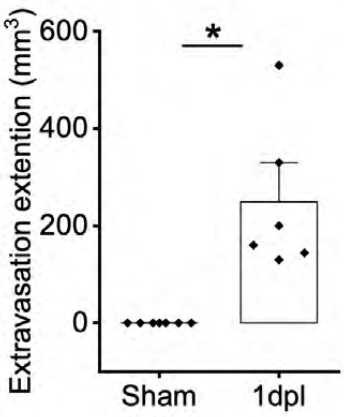

c

	Extravasation	Clasping
EB1	130	3
EB2	160	3
EB3	530	4
EB4	330	4
EB5	200	4
EB6	144	3

d

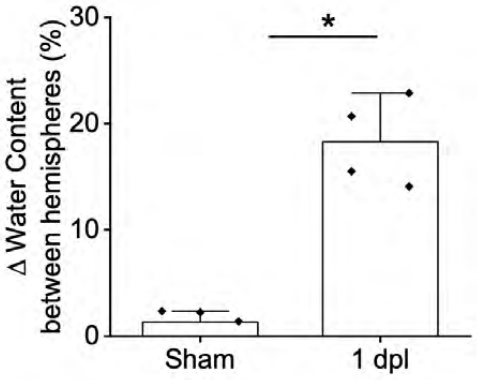

e